Potential Modulation Reflectance of Passivated Type 304 Stainless Steel in Sulfuric Acid Solution

Toshiaki Ohtsuka*, Atsushi Hyono, and Yuki Sasaki

Div. of Material Science and Engineering, Faculty of Engineering, Hokkaido University,

Kita 13 Nishi 8, Kita-ku, Sapporo 060-8628, Japan

Corresponding author; ohtsuka@eng.hokudai.ac.jp

Tel & Fax +81-11-706-6351

Abstract

Potential modulation reflectance (PMR) was applied to passivated type 304 stainless steel covered by a passive oxide film in 0.1 mol dm^{-3} sulfuric acid solution. The ellipsometry measurements showed that the passive oxide film was 1.0 nm thick at the beginning of passivation at 0.1 V vs. Ag/ AgCl and increased to 1.8 nm with potential at 0.9 V in the transpassive region. Under positive bias, the signal intensity of PMR was proportional to the capacitance of the space charge formed in the *n*-type semiconducting passive oxide. The Mott-Schottky type plot was applicable to PMR as well as capacitance. From the plots the oxide film was found to behave as an n-type semiconducting layer. A threshold photon energy of 2.4 eV in the PMR–wavelength relation may correspond to the optical absorption edge of the passive oxide.

Key words: Potential modulation reflectance, Stainless steel, Passive film, ellipsometry, semiconducting oxide.

1. Introduction

Passivation is one of the basic key factors with respect to the corrosion resistance of stainless steels. Passivation is attributed to the formation of a passive film consisting of a few nanometers thick oxide layer on a stainless steel surface. The passive film formed on type 304 stainless steel in acidic solutions has been assumed to be composed of oxides of chromium, iron, and nickel, in which chromium is condensed to a ratio of 40%–60% [1-4], while it was composed of a inner chromium-rich oxide layer and a outer iron-rich oxide layer in neutral and weakly alkaline solutions [4-7]. The detailed dependence of film thickness on potential was estimated by Matsuda *et al.* by ellipsometry [8, 9], who reported a 1–2 nm thick film in the passive potential range; however, a much greater thickness was reported by Toniani *et al*. [9, 10]. It is conceivable that, along with measuring the film growth, Toniani *et al*. also measured the increase in surface roughness, which introduced a relatively large change in ellipsometry parameters, resulting in an overestimation of the thickness of the passive film.

The semiconducting properties of the passive film on stainless steels were studied by various authors, who measured the impedance of passivated steels to estimate capacitance. From the Mott-Schottky plots of capacitance, they evaluated the semiconducting properties of passive films [5, 7, 12-26]. Several authors reported that the semiconductor type of the passive oxide was n-type [12, 13, 15, 16]. On the other hand, since the semiconductor type was assumed to be *n* for Fe_2O_3 [27] and *p* for Cr_2O_3

[27, 28] and the main composition of the passive film on stainless steels was considered to be ferric and chromic oxide or hydroxide, Fereira *et al*. [17-19, 21, 26] and Carmezim *et al*. [23] assumed that the passive film on stainless steels may posses both characteristics. For the Mott-Schottky plot, these authors measured capacitance over a wide range of potential from the passive region to hydrogen evolution region; however, it should be noticed that impedance is very sensitive to the change in film composition and interfacial Faradaic processes such as hydrogen evolution. When the potential of passivated stainless steel is shifted to lower potential, the reductive dissolution of ferric oxide or oxyhydroxide takes place to introduce the loss of ferric elements from the passive film, and hydrogen evolution occurs upon further lowering the potential. The reductive change in the passive film on stainless steel was reported by Piao and Park [30] who measured reflectance from oxide-covered stainless steel in pH 6.8 NaCl solution and found a change in reflectance with increase of cathodic current during a potential sweep from −0.2 V vs Ag/AgCl to more negative potentials. The reductive dissolution of ferric oxide from the artificial ferric–chromic composite oxide was also found by Tanaka *et al*. from the ellipsometric measurement [31]. When the Faradaic redox current is added to the charge-discharge current of the oxide layer at the electrode-solution interface, the interfacial impedance or capacitance was greatly influenced by the redox current, which may conceal the impedance response of the oxide film. The potential for the Mott-Schottky plot should, therefore, be restricted to the range where there are no change in film composition and no Faradaic processes. When the potential for the capacitance measurement is restricted to this range, the

passive film on stainless steel is reported to behave as an *n*-type semiconductor [12, 13, 15, 16].

AC potential modulation reflectance (PMR) or electroreflectance is a surface-sensitive technique for measuring electrode properties. In PMR, reflectance modulated by an AC potential on an electrode is measured as a function of optical wavelength, DC potential, and AC frequency. Upon applying PMR to electrodes covered by a semiconducting oxide layer, reflectance modulation is induced by the change in electronic density within the oxide and/or at the oxide-solution interface [32-35]. When the surface oxide on the electrode is located under the carrier-depression condition, a space charge is formed in the oxide layer and is modulated by the applied AC potential, accompanied by a change in the thickness of the space-charge layer and in the electric field in the space-charge layer [16, 17]. PMR may originate in the change in the space-charge layer. Since thickness and electric field are functions of biased DC potential, as described in the Mott-Schottky plot, PMR also becomes a function of DC potential.

In this paper, we present a precise ellipsometry measurement of the thickness of a passive film on type 304 stainless steel and measure the passive oxide by PMR as well as the electrochemical impedance or capacitance. Furthermore, the basic theory for understanding the results of AC PMR is discussed and the PMR is applied to the passive oxide film. Finally, we compare the results of PMR with capacitance data to examine the semiconducting properties of the passive films on the stainless steel.

2. Experimental

Type 304 stainless steel was used for electrode specimen, which was composed of 18.29 wt% Cr and 8.75 wt% Ni with minor elements of 0.066 wt% C, 0.58 wt% Si, 0.029 wt% P, 0.002 wt% S, 0.82 wt% Mn and 0.14 wt% Mo. The 2-mm-thick specimen was cut into 15 × 15 mm^2 with a small handle for electrical connection. It was mechanically polished by alumina abrasive to a mirror-like surface and then washed ultrasonically in acetone. Before use, the handle part was sealed by an epoxy resin.

The electrolyte solutions were 0.1 mol/dm^3 (M) sulfuric acid and a pH 8.4 borate buffer consisting of a 1:1 mixture of 0.075 M sodium borate and 0.3 M boric acid. The solutions were prepared from analytical grade reagents and milli-Q pure water. The solutions were deaerated by bubbling before use for 2 h with pure nitrogen.

For in situ estimation of the passive oxide film thickness, an automated rotating-analyzer-type ellipsometer was used which was designed in our laboratory and equipped with a He–Ne laser operating at 632.8 nm wavelength [38, 39]. The angle of incidence was 60.0°.

PMR was measured with the apparatus illustrated in Fig. 1. Light from a 450 W xenon lamp was used for the measurement. The light, monochromated by a monochromator, JASCO CN-25N, was polarized by a polarizer on a plane parallel to the incidence plane. In the electrochemical cell with two optical windows, the parallel-polarized (p-polarized) light was reflected by the stainless steel electrode at an

angle of incidence of 60° and the intensity of the reflected light was detected by a photomultiplier. The azimuth of the analyzer located after the electrode was fixed at an angle same to that of the polarizer. A root-mean square (rms) 0.1 V AC potential was superimposed on DC potential and applied to the electrode. AC reflectance dR harmonically modulated by the AC potential was detected by an EG & G 7260 lock-in amplifier. The AC reflectance was divided by AC potential dE and normalized by DC reflectance R_0: (dR/dE)(1/R_0).

AC-potential modulation current (*i.e.*, admittance or inverse of impedance) was measured with an NF Circuit Design 5250 frequency response analyzer. For the measurement, a 0.01 V rms AC potential in the frequency range of 10 mHz–20 kHz was superimposed on DC potential. The potential was measured with an Ag/ AgCl / saturated KCl reference electrode and a platinum sheet was used for the counter electrode.

3. Results

3.1 Voltammogram

Figure 2 shows a voltammogram of type 304 stainless steel measured in a 0.1 M sulfuric acid solution with a potential sweep from −0.4 to 0.9 V (vs. Ag/ AgCl/ saturated KCl) at a sweep rate of 10^{-3} V s^{-1}. The current density (CD) reveals a maximum at −0.01 V and then decreases to 0.7 μA cm^{-2} at 0.05 V. Passivation starts at the potential of 0.05 V, continuing to 0.7 V, and in the passive-potential region, the CD

remains lower than 1 μAcm^{-2}. The CD increases with increasing potential for potentials higher than 0.7 V, where transpassive dissolution may occur with chromate formation.

3.2 Film thickness from ellipsometry measurements

The ellipsometry measurements were performed in the potential region 0.2–0.9 V, in which the stable passive oxide film was expected to form. The results are shown in Fig. 3, where the ellipsometry parameters Ψ (tan Ψ is the relative amplitude ratio of parallel (p)- polarized light to perpendicular (s)- polarized light) and Δ (relative phase retardation between p- and s-polarized light) were plotted with potential change. The potential was initially changed from −0.4 to 0.1 V and then increased to 0.9 V in 0.1 V steps. The individual potentials were held for 1800 s. The Ψ value initially changed by $\delta\Psi = -0.2°$ when the potential changed from −0.4 V in the hydrogen-evolution-potential region to 0.1 V in the passive-potential region and then the Ψ value remained almost constant from 0.1 to 0.9 V. The Δ value changed by $\delta\Delta = -2.5°$ with the formation of the passive film at 0.1 V and then gradually decreased with increasing potential. The increase in change of Δ reflects the film growth with potential.

The film thickness was estimated from changes in Ψ and Δ by using the ordinary Fresnel and Drude reflection equations and assuming a homogeneous-layer model in which a homogeneous oxide layer grows with potential and time. The estimate was conducted with a computer program coded in FORTRAN. For the calculation, the refractive index (i.e., the real part of the complex refractive index, $N = n - jk$) of the oxide film was assumed to be $n = 2.0$ and the extinction index k (*i.e.*, the imaginary

part of the complex refractive index) and thickness d of the oxide film was estimated as a function of $\delta\Psi$ and $\delta\Delta$. Before the calculation, the complex refractive index of the substrate steel was determined from Ψ and Δ for the reduced surface at −0.4 V: on average, $\Psi = 32.953°$ and $\Delta = 148.47°$. For these values of Ψ and Δ, the complex refractive index of the substrate was calculated to be $N = 3.79 - 4.21j$ at 632.8 nm wavelength.

The film thickness calculated from the changes of Ψ and Δ, $\delta\Psi$ and $\delta\Delta$, from the initial reduced surface at −0.4 V is given in Fig. 4. For this calculation, the k value of the film was estimated to range from $k = 0.2$ to 0.5. We also plot in Fig. 4 the CD acquired after 1800 s of potentiostatic oxidation at the individual potentials. The resulting thickness was about $d = 1.0$ nm at the initial passivation at 0.1 V and then increased to 1.8 nm with increasing potential at the beginning of the transpassive potential region.

3.3 Spectrum of potential modulation reflectance of passive oxide

The PMR spectrum was measured for a passive film formed in 0.1 M sulfuric acid solution and the result is shown in Fig. 5. For this figure, PMR was measured at 0.41 V in a pH 8.4 borate solution at a frequency of 13 Hz after passive oxide formation for 1800 s at 0.85 V in 0.1 M sulfuric acid solution. PMR is a complex number and accordingly the absolute value and phase retardation of PMR were plotted in Fig. 5. For the PMR measurement, we replaced sulfuric acid with a neutral borate solution for the following reason: in acidic solutions, the passive oxide may be sensitive to change in

potential because the dissolution rate of the film is relatively high. Since in this study, we adopted a 0.1 V_{rms} AC potential to provide a detectable PMR signal, the film may possibly have been affected by the relatively large potential modulation. In the neutral borate solution, the film is much more stable because dissolution rate of the film is much lower and the film growth is assumed to be a slow response to changes in potential. We believe that the passive film is frozen in the neutral solution without significant changes in thickness or composition. However, to avoid further growth of the passive film in the pH 8.4 borate solution, the potential in the borate solution for the PMR measurement was shifted by -0.059ΔpH (V), where ΔpH is the pH difference between 0.1 M sulfuric acid solution (pH 0.9) and borate buffer solution (pH 8.4).

The phase retardation shown in Fig. 5 is about $\theta = 170°$, and therefore, reflectance was inversely modulated by potential; that is, reflectance decreased with increasing potential. The PMR amplitude was almost constant for wavelengths longer than 520 nm but increased as wavelength decreased below 520 nm.

3.4 Dependence of PMR on potential decrease

To investigate the dielectric or semiconducting properties of the passive oxide film formed at a specific formation potential E_f, the capacitance of the electrode covered by the film was measured as a function of potential by various authors [4-26]. Usually, the potential is shifted from the formation potential to a lower potential and capacitance or impedance is measured as a function of the decrease in potential. In the acidic solution, however, the potential decrease in the sulfuric acid solution during the measurement of

the capacitance–potential (*C–E*) relation possibly induces a change in the oxide film thickness and composition because of the relatively high dissolution rate.

To measure the *C–E* relation, we replaced the sulfuric acid solution with a pH 8.4 borate buffer solution, as done in the preceding section. Figure 6 shows the CD–potential relation acquired in the pH 8.4 borate buffer solution at a sweep rate of 2×10^{-3} V s^{-1} after passivation at $E_f = 0.85$ V for 1800 s in 0.1 M sulfuric acid solution. To avoid further growth of the passive film in the pH 8.4 borate solution, the starting potential in the borate solution was shifted to $E_f - 0.0591\Delta$pH (V). In the potential range from 0.42 to −0.30 V, the CD was less than −0.2 μA/cm^2; hence, we believe that the oxide film did not change significantly.

A relatively large cathodic CD of 1 μA/cm^2 was observed with potentials below −0.3 V. In this potential range, reduction dissolution of Fe(III) oxide or hydroxide to Fe(II) ion was expected to occur [15]; therefore, the composition change might have started at −0.3 V. To investigate the *C–E* relation, the data in the potential region below −0.3 V should be avoided. We discuss the *C–E* relation in the potential range from E_f– 0.059 ΔpH (V) to −0.3 V in the borate buffer solution for the film formed at E_f in the sulfuric acid solution.

Figure 7 shows the impedance response plotted against frequency (i.e., Bode plot) for steel covered by a passive oxide film formed at 0.85 V in 0.1 M sulfuric acid solution. Impedance was measured in a borate solution at a potential of 0.41 V to which the potential was shifted from $E_F = 0.85$ V in 0.1 M sulfuric acid by $E_f - 0.059\Delta$pH. The plot indicates that the electrode with the passive film could be represented by an

equivalent circuit (Fig. 8(A)) consisting of a series connection between a solution resistance R_s and a parallel circuit of film resistance R_f and film capacitance C_f. From the low-frequency limit, the film resistance is calculated to be greater than 10^6 Ω cm^2.

For the *C–E* relation in the Mott-Schottky plot, a specific frequency should be selected and impedance should be measured as a function of decreasing potential at the selected frequency. We adopted 13 Hz as the fixed frequency, at which the circuit could be approximated as a series connection between the solution resistance and the film capacitance (Fig. 8(B) because the film resistance R_f was much larger than the impedance of $1/(j2\pi fC_f)$ at f = 13 Hz and the selected angular frequency, ω (=$2\pi f$), are much larger than inverse of the time constant of R_f-C_f parallel circuit, which is seen in Fig. 7. With the approximated circuit as shown in Fig. 8(B), the film capacitance was calculated from the imaginary part of complex impedance, Im(Z), at f = 13 Hz and C_f = $1/ [2\pi f \mathrm{Im}(Z)]$. Since the selected frequency is seen to be much smaller than the inverse of the other time constant of R_s-C_f series connection in Fig. 6, the most of AC potential imposed to the electrode is borne in the oxide layer.

PMR can be related to the film capacitance, as described in the discussion section below. The dependence of PMR on potential was also measured at f = 13 Hz in the pH 8.4 borate solution for the oxide films formed in 0.1 M sulfuric acid solution. Figure 9 shows a PMR–potential relation measured at three wavelengths of λ = 350, 400, and 450 nm during potential sweeps from 0.41 to −0.50 V at a sweep rate of 10^{-4} V s^{-1}. Although PMR is a complex number, only the absolute value (amplitude) of PMR is plotted in Fig. 9. Phase retardation with respect to AC potential was about θ = 175° to

155° for potentials between 0.4 and −0.1 V. PMR at λ = 400 and 450 nm was less than 10^{-3} V^{-1} and depended weakly on potential. PMR at λ = 350 nm, however, exhibited a clear dependence on potential, increasing with decreasing potential.

In Fig. 10, the PMR response at 350 nm wavelength to the potential is compared with the capacitance response. The complex capacitance was calculated from the complex impedance Z using $C_{CMX} = 1/(2\pi fZ)$ at f = 13 Hz. The both amplitudes of C_{CMX} and PMR increased with decreasing potential and, however, the phase shift of C_{CMX} changed from -20° to -25°, while that of PMR from 170° to 120°. From the comparison between the phase shifts of C_{CMX} and PMR, it is found that PMR is inversely modulated with respect to complex capacitance; that is, positive charge accumulation in the film induces a decrease in reflectance.

4. Discussion

4.1 Potential modulation of electrode covered by semiconducting passive oxide

We now discuss the AC modulation of the electrode covered by an oxide film with dielectric and/or semiconducting properties in view of elucidating the relation between capacitance and PMR.

In Fig. 11, a model is illustrated in which the electrode is covered by an *n*-type semiconducting oxide film and biased by a positive potential (*i.e.*, reverse biased for the n-type semiconducting electrode). When an AC bias is applied to the passive-film-covered electrode, AC impedance is defined as the ratio of AC potential to

AC current:

$$Z = \mathrm{d}E/\mathrm{d}i. \qquad (1)$$

For a thin, reverse-biased *n*-type semiconducting oxide film, AC current can be related to the change in the space charge in the depression layer. We now define the complex capacitance C_{CMX} as

$$C_{CMX} = \mathrm{d}Q/\mathrm{d}E = (1/j\omega)(\mathrm{d}i/\mathrm{d}E) = (1/j\omega)(1/Z), \qquad (2)$$

where $\omega = 2\pi f$ is angular frequency. Complex capacitance corresponds to charge accumulation and depression in the circuit. When one approximates the circuit by an equivalent circuit consisting of a series connection between a solution resistance R_s and a film capacitance C_f, as described earlier, the complex capacitance takes the following form:

$$1/C_{CMX} = (1/C_f) + j\omega R_s. \qquad (3)$$

The change in reflectance with AC potential may be assumed to originate in a change in electron density in the film. In positive-biased *n*-type semiconducting oxide, the thickness of the space-charge layer is harmonically modulated with AC potential, so the electron density in the region between the space-charge layer and the inner layer is also modulated. Because the change in the electron density possibly induces a reflectance change, PMR is harmonically proportional to the complex capacitance:

$$\mathrm{d}R/\mathrm{d}E = K(\mathrm{d}Q/\mathrm{d}E) = KC_{CMX}, \qquad (4)$$

where K is a constant relating modulation reflectance to charge. PMR and C_{CMX} are assumed to be modulated with the same phase retardation with respect to AC potential, although the PMR and C_{CMX} phases are reversed with respect to each other.

The phase retardations of both modulation reflectance and complex capacitance can be analyzed by considering a simplified equivalent circuit consisting of a series connection of R_s and C_f (Fig. 8(B)). Because reflectance was approximately inversely proportional to charge in the space charge as shown in Fig. 10, the reflectance is assumed to be directly modulated by AC potential (dE_{sc}) applied in the space-charge layer of the oxide film. Thus, the experimentally measured PMR can be described as follows:

$$\mathrm{d}R/\mathrm{d}E = (\mathrm{d}R/\mathrm{d}E_{sc})(\mathrm{d}E_{sc}/\mathrm{d}E) \qquad (5)$$

where $(\mathrm{d}R/\mathrm{d}E_{sc})$ becomes a real number. The equivalent circuit shows that the relation between dE_{sc} in the space-charge layer, and dE exactly imposed on the electrode from the outer circuit takes the form

$$\mathrm{d}E_{sc}/\mathrm{d}E = (j\omega C_f)^{-1}/[R_s + (j\omega C_f)]^{-1}$$

$$= \{1/[1 + (\omega/\omega_0)^2]\}[1 - j(\omega/\omega_0)] \qquad (6)$$

where ω_0 is the specific angular frequency of series R_s–C_f circuit:

$$\omega_0 = 1/(R_s C_f) = 1/\tau \qquad (7)$$

with τ being the time constant of the circuit.

The quantity $\mathrm{d}R/\mathrm{d}E$ is a complex number that can be described as follows:

$$\mathrm{d}R/\mathrm{d}E = (\mathrm{d}R/\mathrm{d}E_{sc})\ \{1/[1 + (\omega/\omega_0)^2]\}\ [1 - j(\omega/\omega_0)] \qquad (8)$$

If the ratio ω/ω_0 is much smaller than 1 (*i.e.*, the frequency at which PMR is measured is much smaller than the specific frequency ω_0 of the circuit), then the following approximation holds:

$$\mathrm{d}R/\mathrm{d}E \simeq \mathrm{d}R/\mathrm{d}E_{sc}. \qquad (9)$$

In this case, the measured dR/dE is not a complex number but a real number. If the ratio ω/ω_0 is not much smaller than 1, then dR/dE becomes a complex number, as having been shown in Fig. 10, and phase retardation θ is given by

$$\theta = -\arctan(\omega/\omega_0) \text{ or } [180° - \arctan(\omega/\omega_0)] \qquad (10)$$

For the complex capacitance C_{CMX}, a similar approximation may be performed:

$$C_{CMX} = C_f\{1/[1+(\omega/\omega_0)^2]\}\ [1 - j(\omega/\omega_0)]. \qquad (11)$$

The phase retardation of the PMR in Fig. 10 is about 160° over the potential range of −0.2 to 0.4 V, and thus (ω/ω_0) is estimated to be $\omega/\omega_0 = 0.36$ from Equation (8). From the measurement frequency at f = 13 Hz, the specific frequency can be calculated to be $\omega_0 = 230\ s^{-1}$. On the other hand, the specific frequency estimated from the Bode plot of impedance (Fig. 7) is about $\omega_0 = 750\ s^{-1}$. The difference in the specific frequency may be derived by neglecting the presence of the constant-phase element in the equivalent circuit. The impedance Bode plot in Fig. 7 shows that d(log |Z|)/d(log f) is not 1 but is slightly smaller, so the constant-phase element would be used for a precise simulation by the equivalent circuit.

The phase retardation of PMR is different from that of C_{CMX} for potentials more negative than −0.1 V, as shown in Fig. 10, where the phase retardation of PMR changes from −20°(+160°) at −0.1 V to −60°(+180°) at −0.4 V, although the phase retardation of C_{CMX} varies from −20° to −27°. This discrepancy is not understood at present. A possible explanation is that modulation reflectance may be influenced by the surface states on the oxide film and/or the change in ionic density in the electric double layer at the solution side.

In Fig. 12, the relation between PMR and C_{CMX} is described using the ratio Real (PMR)/real(C_{CMX}), where the Real(PMR) and Real(C_{CMX}) are real parts of the complex numbers. The real (C_{CMX}) is related with the film capacitance, *i.e.*, the space charge capacitance from equation (11),

$$\text{Real}(C_{CMX}) = C_f\{1/[1+(\omega/\omega_0)^2]\} \quad (12)$$

The Real (PMC) is also related with a modulation reflectance in the space charge layer from equation (8),

$$\text{Real(PMR)} = (dR/dE_{sc})\ (1/R_0)\{1/[1 + (\omega/\omega_0)^2]\} \quad (13)$$

The ratio of the real parts can be described as the following way,

$$\text{Real (PMR)/ real}(C_{CMX}) = \quad (dR/dE_{sc})\ (1/R_0) / C_f$$

From Fig. 12, the ratio of the real parts was almost constant at -140 (±30) C^{-1} cm^2 in the potentials from 0.4 V to -0.4 V. The ratio indicates that a charge accumulated in the space charge induces a constant change of amplitude of reflectance modulation. When one considers the exact charging that occurs experimentally, a positive charge density of 1 μC cm^{-2} in the space-charge layer corresponds to a change in reflectance $dR/R_0 = -1.4 \times 10^{-4}$.

4.2 Spectroscopic response of modulation reflectance

When the film does not absorb light, modulation reflectance should not be strong. If one assumes that, because of the smaller electronic density in the space-charge layer or depression layer, the absorption coefficient in the space-charge layer is different from that of the original oxide, then the modulation of depth of the

space-charge layer by an AC potential will give modulation reflectance. Because one can consider that the reflectance change that results from the space-charge modulation in the oxide may be proportional to the intensity of optical absorption in the original oxide film, the modulation reflectance spectrum may possibly reflect the absorption properties of the film. From Fig. 5, we find that, starting at 520 nm wavelength, modulation reflectance increases with decreasing wavelength, whereas it is almost constant at 4.3×10^{-4} V^{-1} above 520 nm wavelength. Under the assumption that modulation reflectance is proportional to the intensity of optical absorption, the absorption edge would exist at the threshold wavelength of 520 nm (photon energy of 2.4 eV). Because the photo-induced current from the photo-electrochemical measurement starts to appear from almost the same photon energy [1], we conclude that the threshold wavelength (or photon energy) found in this study may correspond to the optical absorption edge.

4.3 Mott-Schottky-type plot

The inverse of capacitance is proportional to the depression layer thickness; that is, the capacitance of the space-charge layer in an *n*-type semiconductor oxide under reverse bias obeys the Mott-Schottky relation:

$$C_{sp}^{-2} = [2/(\varepsilon\varepsilon_0 N_D e)](E - E_{FB} - kT/e) \qquad (14)$$

where C_{sp} represents the space-charge capacitance, N_D is the donor density, ε is the dielectric constant, ε_0 is the vacuum permittivity, and E_{FB} is the flat-band potential. Because the space-charge capacitance corresponds to the film capacitance C_f, which

can be estimated from C_{CMX} in equation (3). If the Real(PMR) is assumed to be proportional to the film capacitance, PMR as a function of E must also follow the relation similar as the Mott-Schottky equation. Figure 13 shows C_f^{-2} vs. E and $\{\text{Real}[(dR/dE)(1/R_0)]\}^{-2}$ vs. E for λ = 350 nm, measured at f = 13 Hz, and it is seen that both follow a linear relation in potentials from 0.0 V to -0.3 V and the relation indicates that the passive oxide layer on the type 304 stainless steel posses n-type semiconducting property. This result allows us, by extrapolating the linear range of both curves to the potential axis, to estimate the flat-band potential. From the potential of -0.36 V extrapolated on the C_f^{-2} vs. E plot, the flat-band potential is estimated to be about −0.34 V vs. Ag/ AgCl/ saturated KCl and is in agreement with the potential extrapolated on the $\{\text{Real}[(dR/dE)(1/R_0)]\}^{-2}$ vs. E plot. From the slope of C_f^{-2} vs. E, the donor density of the oxide film is estimated to be 8×10^{20} cm^{-3} under the assumption ε = 15.6 [14,15] .

The results shown in Fig. 12 indicate that the space-charge layer is optically observable with the PMR technique.

Conclusion

The ellipsometry results indicate that the passive oxide film on type 304 stainless steel is 1.0 nm thick at the beginning of passivation at 0.1 V vs Ag/AgCl saturated KCl and increases to 1.8 nm with potential at 0.9 V, the point at which transpassive dissolution starts.

PMR of passivated stainless steel in 0.1 M sulfuric acid solution can be

explained by modeling it as an *n*-type semiconducting oxide film under positive bias. In the model the AC potential modulates the space charge in the depression layer and PMR originates in the modulation of the space charge. This model was experimentally confirmed from a proportional relation between PMR and space-charge capacitance.

From the spectroscopic PMR measurement, the optical absorption edge of the passive oxide was found to be 520 nm wavelength (photon energy of 2.4 eV).

The same relation to the Mott-Schottky plot of C_{sp}^{-2} vs. E was established for the PMR, *i.e.*, $[(dR/dE)(1/R_0)]^{-2}$ vs. E. From the plots, the flat band potential of n-type semiconducting oxide film on the stainless steel was found to be about −0.34 V.

References

(1) S. Fujimoto, T. Yamada, T. Shibata, J. Electrochem. Soc., 145 (1998) L79.

(2) I. Olefjord, Materials Sci. and Eng., 42 (1980) 161.

(3) V. Maurice, W. P. Yang, P. Marcus, J. Electrochem. Soc., 145 (1998) 909.

(4) G. Lorang and M. Da Cunha Belo, A. M. P. Simões, M. G. S. Ferreira, J. Electrochem. Soc., 141 (1994) 3347.

(5) N. E. Hakiki, M. Da Cunha Belo, A. M. P. Simões, M. G. S. Ferreira, J. Electrochem. Soc., 145 (1998) 3821.

(6) M.J. Carmezim, A.M. Simoes, M.F. Montemor, M. da Cunha Belo, Corros. Science, 47 (2005) 581.

(7) L. Freirea, M. J. Carmezima, M. G. S. Ferreira, M.F. Montemor, Electrochim. Acta,

55 (2010) 6174.

(8) S. Matsuda, K. Sugimoto, Y. Sawada, Transact. JIM, 18 (1977) 66.

(9) K. Sugimoto, S. Matsuda, Mater. Sci. Eng., 42(1990) 181.

(10) A. Bose, M. K. Totiani, (1999) Ind. J. Eng. Mater. Sci., 6 !999) 213.

(11) S. V. Phadnis, M. K. Toniani, D. Bhattachaya, Transact. Inst. Metal. Finish. 76 (1998) 235.

(12) A. Di Paola, Electrochim. Acta, 34 (1989) 203.

(13) A. M. P. Simoes, M. G. S. Ferreira, B. Rondot, M. da Cunha Belo, J. Electrochem. Soc., 137 (1990) 82.

(14) A. M. P. Simoes, M. G. S. Ferreira, B. Rondot, M. da Cunha Belo, Electrochim. Acta, 36 (1991) 315..

(15) R. Babic and M. Metikos-Hukovic, J. Electroanal. Chem., 358 (1993) 143.

(16) J.-P. Petit, A. Antoni, B. Baroux, European Federation of Corrosion Publication, No. 12, Modifications of passive films, Ed. By P. Marcus, B. Baroux and M. Keddam, The Institute of Metals (1994) 9.

(17) M. da Cunha Belo, R. Rodot, C. Compere, M. F. Montemor, A. M. P. Simoes, M. G. S. Ferreira, Corros. Sci., 40 (1998) 481.

(18) M. G. S. Ferreira, A. M. P. Simoes, C. Compere, B. Rondot, M. da Cunha Belo, Materials Sci. Forum,289-292 (1998) 887.

(19) N. E. Hakiki, M. da Cunha Belo, A. M. P. Simoes, M. G. S. Ferreira, J. Electrochem. Soc., 145 (1998) 381.

(20) H. Tsuchiya, S. Fujimoto, T. Shibata, J. Electrochem. Soc., 151 (2004) B39.

(21) M. G. S. Ferreira, N. E. Hakiki, G. Goodlet, S. Faty, A. M. P. Simões, M. Da Cunha Belo, Electrochim. Acta, 46 (2001) 3767,

(22) F. Gaben, B. Vuillemin, and R. Oltra, J. Electrochem. Soc., 151 (2004) B595.

(23) M. J. Carmezim, A.M. Simões, M.F. Montemor and M. Da Cunha Belo, Corros. Sci., 47 (2005) 581.

(24) Z. Feng, X. Cheng, C. Dong, L. Xu. X. Li, Corros. Sci., 52 (2010) 3646.

(25) A. Fattah-alhosseini, M.A. Golozar, A. Saatchi, K. Raeissi, Corros. Sci., 52 (2010) 205.

(26) L. Freire, M. J. Carmezim, M. G. S. Ferreira, M.F. Montemor, Electrochim. Acta, 55, (2010) 6174.

(27) K. Azumi, T. Ohtsuka and N. Sato, J. Electrochem. Soc., 134 (1987) 1352.

(28) S. Virtanen, P. Schmuki, H. Bohni, P. Vuoristo, T. Mantyla, J. Electrochem. Soc. 142 (1995) 3067.

(29) D-S. Kong, S-H. Chen, C. Wang, W. Yang, Corros. Sci., 45 (2003) 747.

(30) T. Piao and S-M. Park, J. Electrochem. Soc., 144 (1997)3371.

(31) S. Tanaka, N. Hara, K. Sugimoto, Mater. Sci. and Eng. A198, (1995) 63.

(32) N. Hara, K. Sugimoto, J. Electrochem. Soc., 142 (1991) 3067.

(33) N. Hara, K. Sugimoto, Transact. JIM, 24 (1983) 236.

(34) K. Sugimoto, M. Sato, S. Tanaka, N. Hara, J. Electrochem. Soc. 140 (1993) 1586.

(35) A. Kawai, G.Gutierrez, J. Electroanal. Chem., 395 (1995) 243

(36) D. J. Wheeler, B. D. Cahan, C. T. Chen, E. Yeager, (1978) Passivity of Metals, Ed by R. P. Frankenthal and J. Kruger, the Electrochem Soc Inc, (1978) 546.

(37) D. J. Blackwood, C. M. Peter, Electrochim. Acta 35, (1990), 1073.

(38) T. Ohtsuka, Y. Sato, K. Uosaki, Langmuir, 10 (1994) 3658

(39) T. Ohtsuka, Denki Kagaku, 60 (1992) 1123.

Figure Captions

Fig. 1 Scheme of apparatus for measuring potential modulation reflectance (PMR). E; DC potential, dE; AC modulation potential, i; current, R_0; DC reflectance, and dR; AC modulated reflectance.

Fig. 2 Current density i vs potential E for type 304 stainless steel in 0.1 M sulfuric acid solution from −0.4 to 0.9 V at a sweep rate of 10^{-3} V/s.

Fig. 3 Change in ellipsometric parameters Ψ and Δ during stepwise change in potential from E = −0.4 to 0.9 V in 0.1 M sulfuric acid solution. The individual potentials were held for 1800 s.

Fig. 4 Thickness d of passive oxide film and passive current density i as a function of potential E in 0.1 M sulfuric acid solution. The thickness was estimated from the results shown in Fig. 3. The current density was taken after potentiostatic oxidation for1800 s.

Fig. 5 PMR spectrum of passive oxide on stainless steel formed at 0.85 V vs. Ag/ AgCl in 0.1 M sulfuric acid solution. PMR was measured at 0.41 V in pH 8.4 borate solution at 13 Hz.

Fig. 6 Current density i vs potential E for passivated stainless steel measured in pH 8.4

borate solution from $E = 0.45$ to −1.0 V at a sweep rate of $v = 2 \times 10^{-3}$ V s^{-1}. Passivation was performed at $E = 0.85$ V for 1.800 s in 0.1 M sulfuric acid solution before the potential sweep measurement.

Fig. 7 Impedance ($|Z|$, θ) of passivated stainless steel measured at 0.41 V in pH 8.4 borate solution. Passivation was performed at $E = 0.85$ V for 1800 s in 0.1 M sulfuric acid solution before the impedance measurement.

Fig. 8 (A) Equivalent circuit corresponding to the impedance response in Fig. 7 and (B) approximated circuit of the impedance response at a frequency of f = 13 Hz. The frequency, $\omega (= 2\pi f)$ is; $(1/R_f C_f) << \omega < (1/R_s C_f)$.

Fig. 9 PMR $(dR/dE)(1/R_0)$ vs. potential E for passivated stainless steel measured at wavelengths of λ = 350, 400, and 450 nm in pH 8.4 borate solution during potential sweep from 0.41 to −0.5 V at a sweep rate of 10^{-4} V s^{-1}. Passivation was performed at $E = 0.85$ V for 1800 s in 0.1 M sulfuric acid solution before the PRM measurement.

Fig. 10 Comparison between complex capacitance (C_{CMX}) and PMR $(dR/dE)(1/R_0)$ at λ = 350 nm as a function of potential in pH 8.4 borate solution during a potential sweep from 0.41 to −0.5 V. Passivation was performed at $E = 0.85$ V for 1800 s in 0.1 M sulfuric acid solution.

Fig. 11 Schematic model of *n*-type semiconducting oxide film under reverse bias (anodic potential against flat-band potential). The space charge and its thickness changes with applied AC potential.

Fig. 12 Ratio of real part of PMR to that of complex capacitance, Real[$(dR/dE)(1/R_0)$]/ Real[C_{CMX}], measured in pH 8.4 borate solution during potential sweep from 0.41 to −0.5 V. Passivation was performed at E = 0.85 V for 1800 s in 0.1 M sulfuric acid solution.

Fig. 13 Mott-Schottky-type plot of C_{sp}^{-2} vs. E and $\{\text{Real}[(dR/dE)(1/R_0)]\}^{-2}$ vs. E at λ = 350 nm measured in pH 8.4 borate solution during potential sweep from 0.41 to −0.5 V. Passivation was performed at E = 0.85 V for 1800 s in 0.1 M sulfuric acid solution.

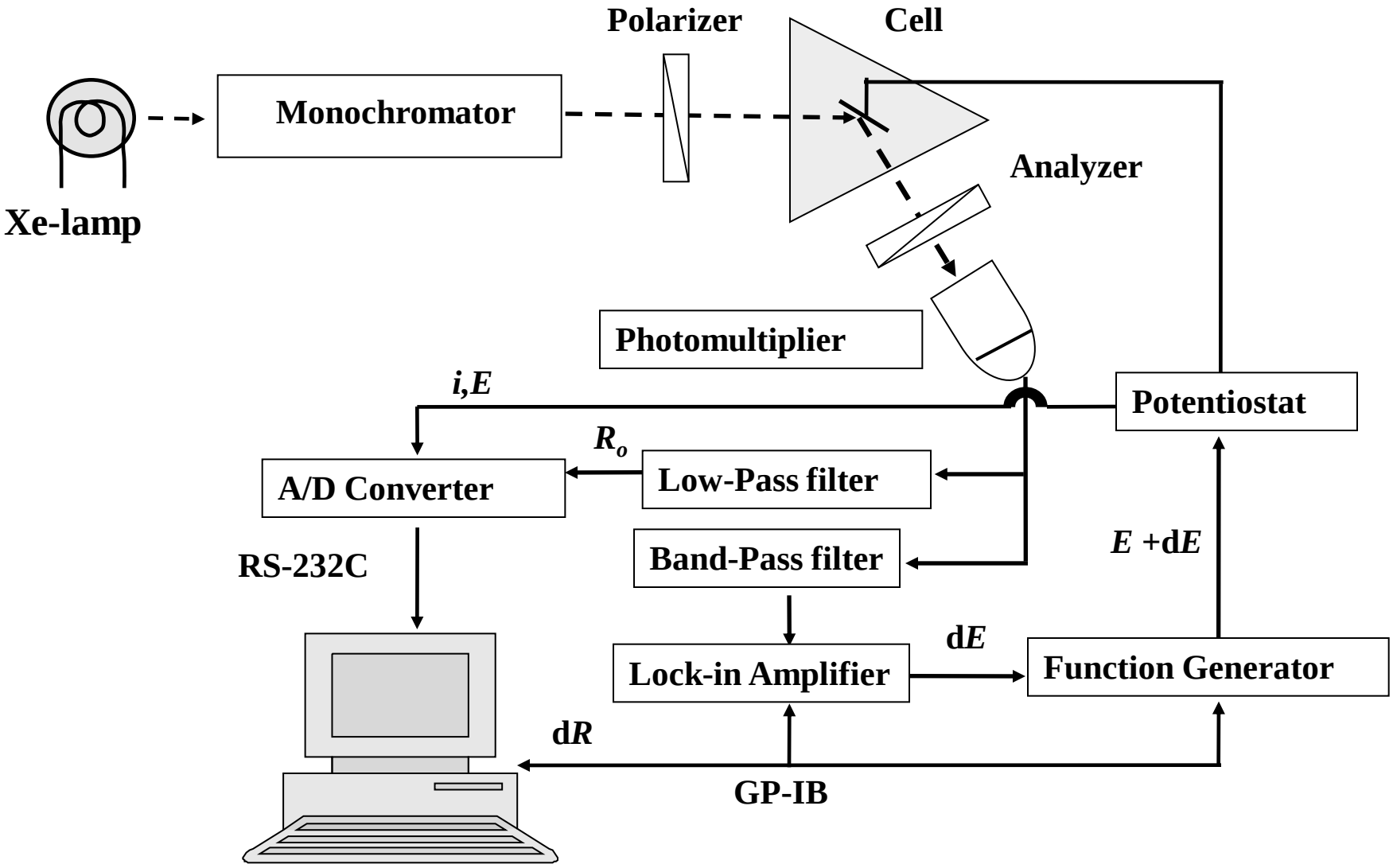
Polarizer
Cell
Monochromator
Xe-lamp
Analyzer
Photomultiplier
i,E
Potentiostat
R_o
A/D Converter
Low-Pass filter
RS-232C
Band-Pass filter
E +dE
dE
Lock-in Amplifier
Function Generator
dR
GP-IB

Fig. 1.

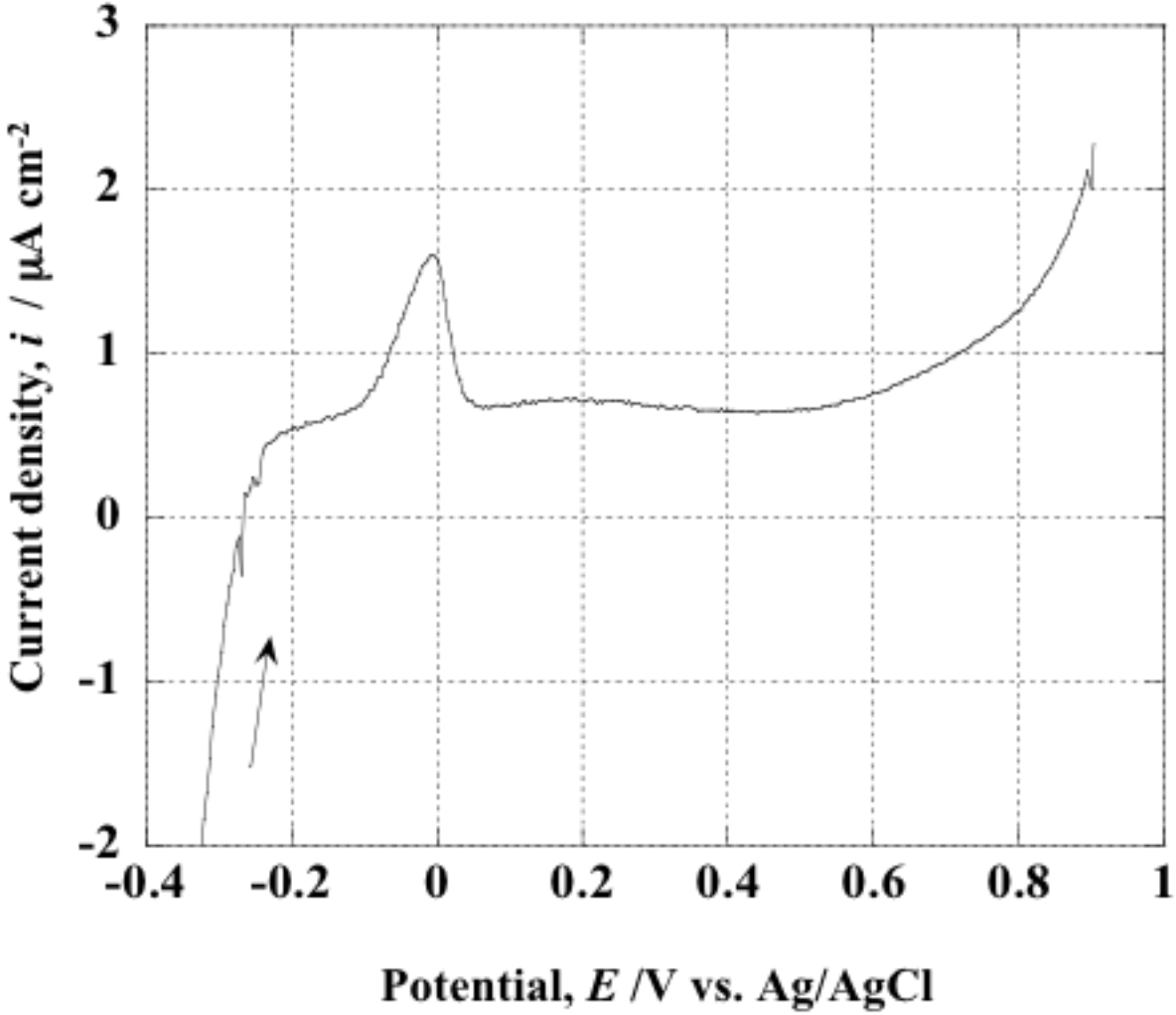
Current density, i / μA cm-2
3
2
1
0
-1
-2
-0.4
-0.2
0
0.2
0.4
0.6
0.8
1
Potential, E /V vs. Ag/AgCl

Fig. 2

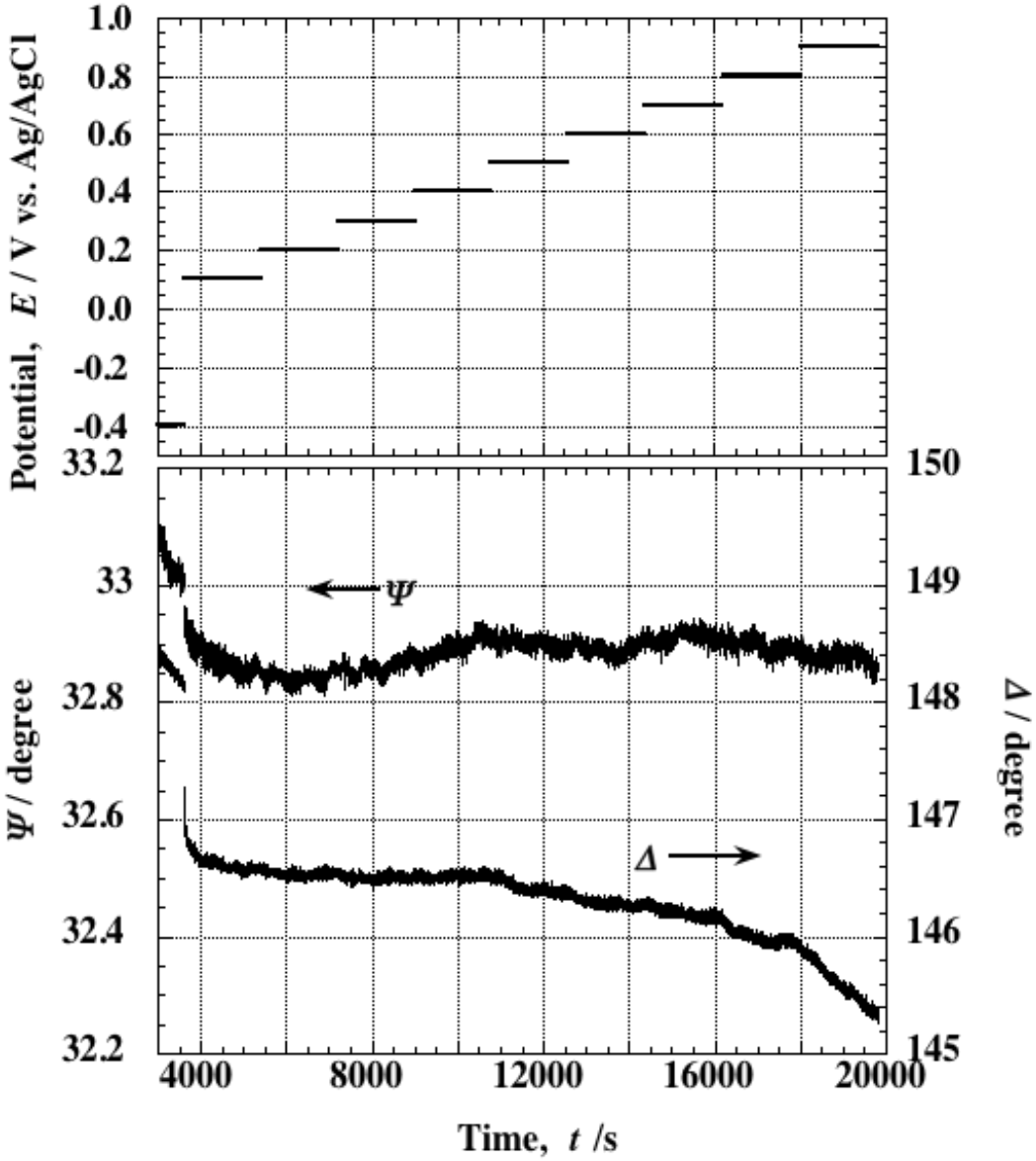
Potential, E / V vs. Ag/AgCl
1.0
0.8
0.6
0.4
0.2
0.0
-0.2
-0.4
Ψ / degree
33.2
33
32.8
32.6
32.4
32.2
Δ / degree
150
149
148
147
146
145
Ψ
Δ
4000
8000
12000
16000
20000
Time, t /s

Fig. 3

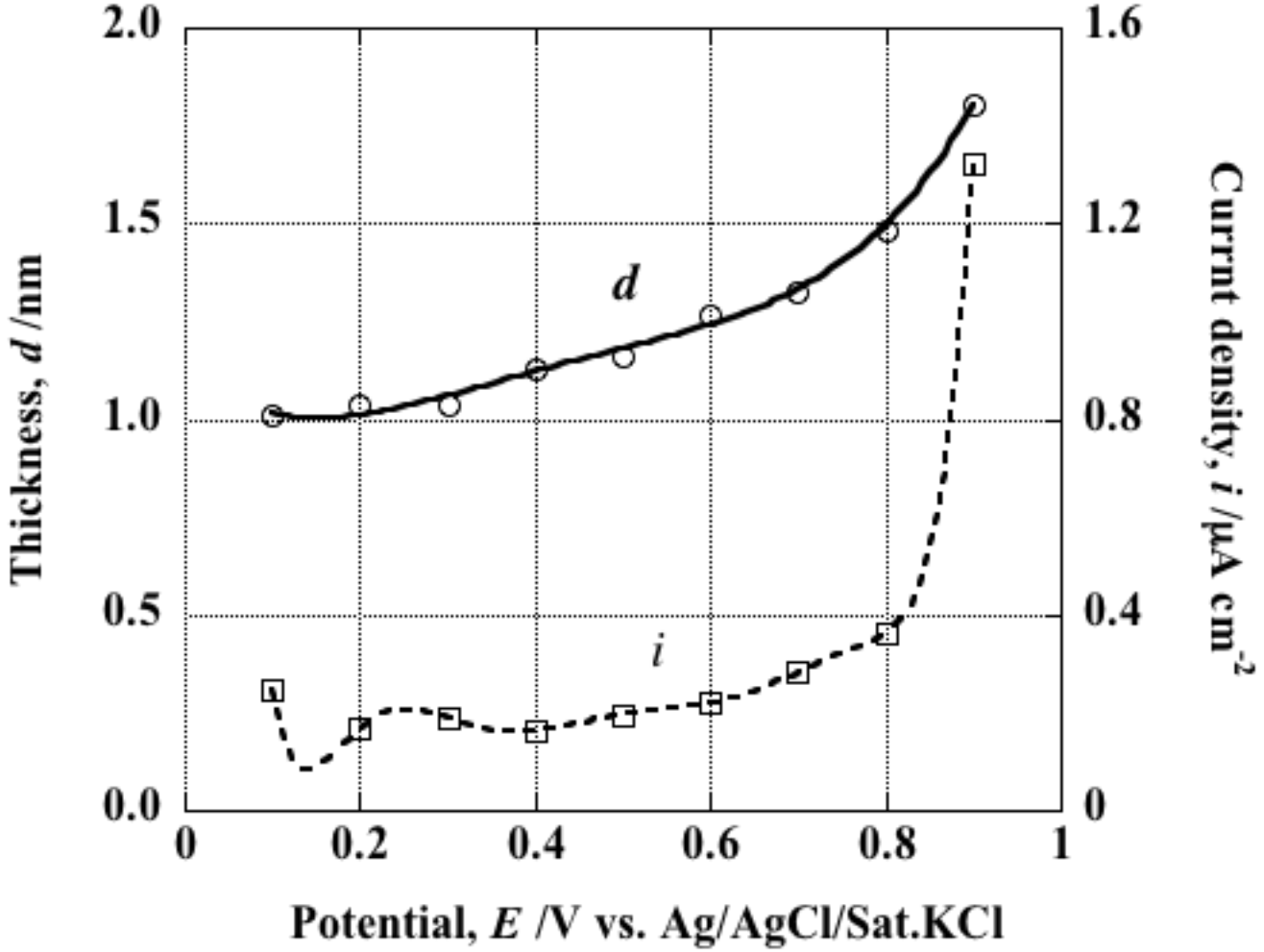
2.0
1.5
1.0
0.5
0.0
1.6
1.2
0.8
0.4
0
0
0.2
0.4
0.6
0.8
1
d
i
Thickness, d /nm
Currnt density, i /μA cm-2
Potential, E /V vs. Ag/AgCl/Sat.KCl

Fig. 4

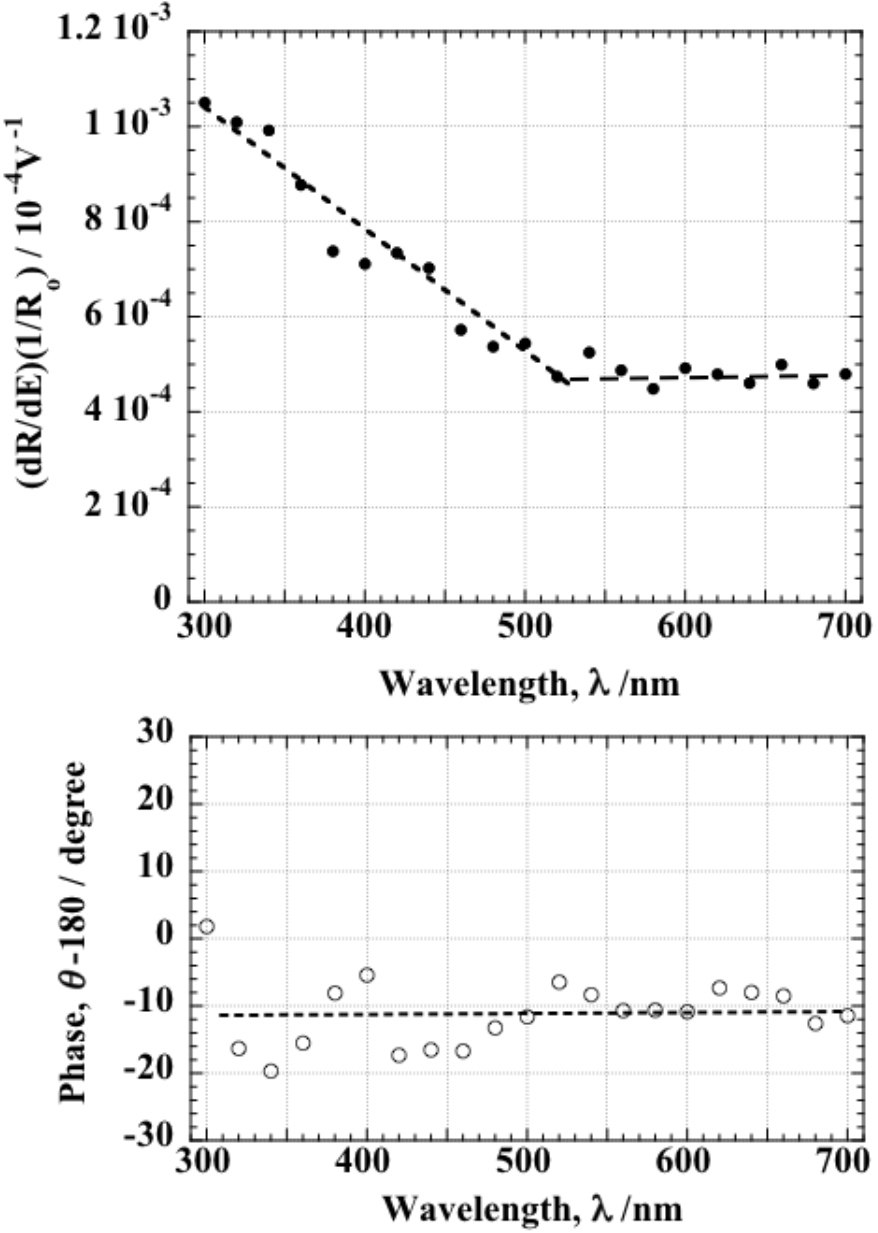
1.2 10^-3
1 10^-3
8 10^-4
6 10^-4
4 10^-4
2 10^-4
0
(dR/dE)(1/R_o) / 10^-4V^-1
300
400
500
600
700
Wavelength, λ /nm
30
20
10
0
-10
-20
-30
Phase, θ-180 / degree
300
400
500
600
700
Wavelength, λ /nm

Fig. 5

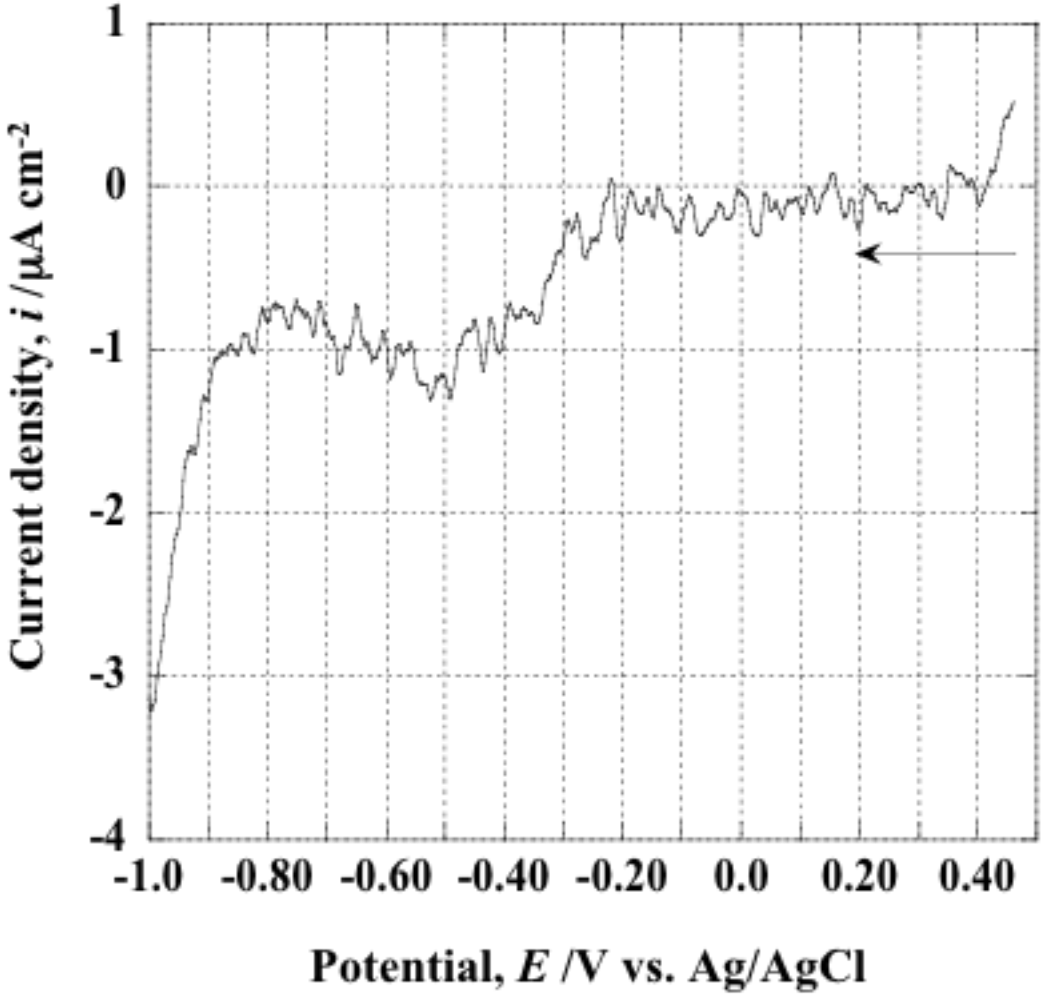
1
0
-1
-2
-3
-4
Current density, i /μA cm-2
-1.0
-0.80
-0.60
-0.40
-0.20
0.0
0.20
0.40
Potential, E /V vs. Ag/AgCl

Fig. 6

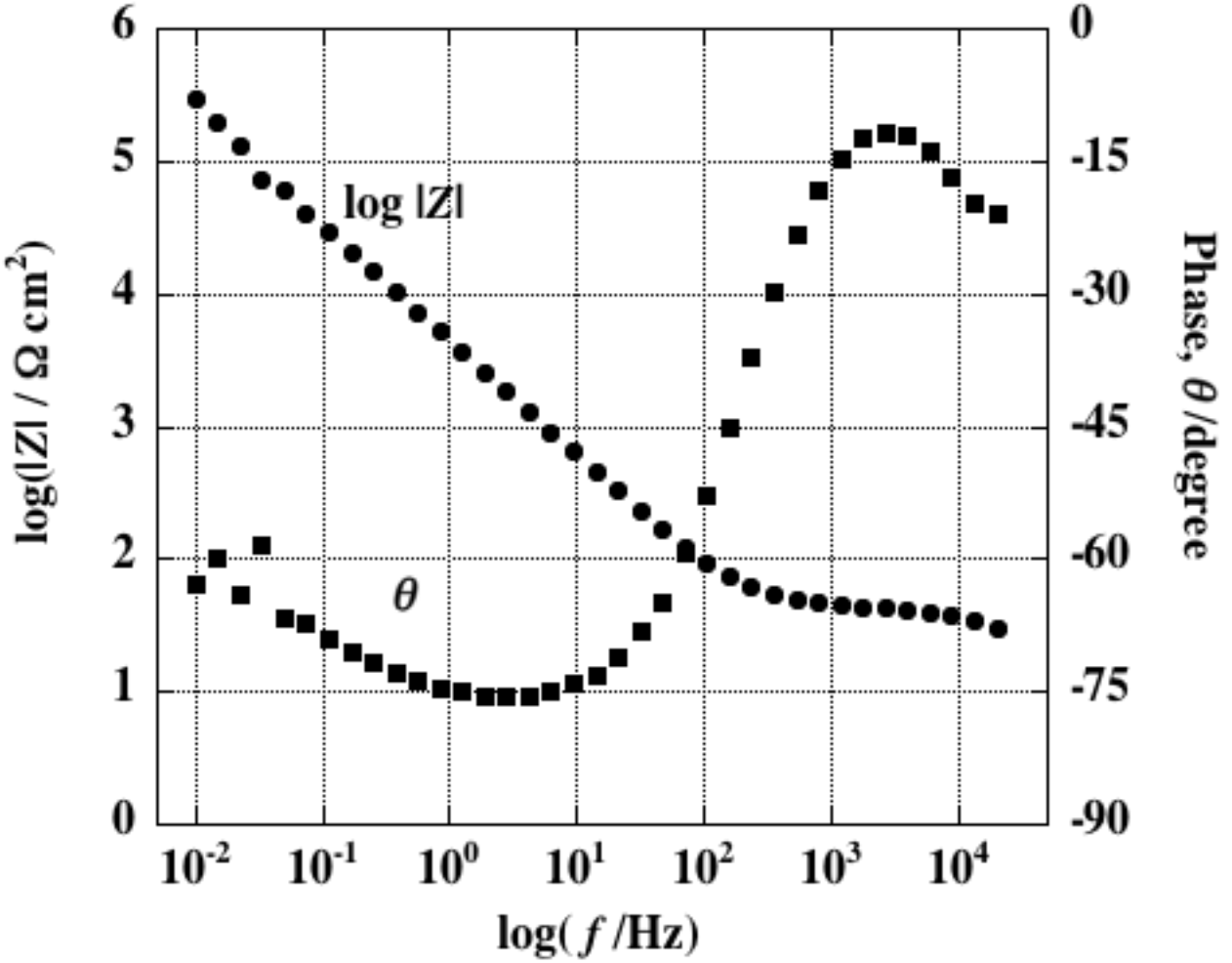
log |Z|
θ
log(|Z| / Ω cm²)
Phase, θ /degree
log(f /Hz)
6
5
4
3
2
1
0
0
-15
-30
-45
-60
-75
-90
10⁻²
10⁻¹
10⁰
10¹
10²
10³
10⁴

Fig. 7

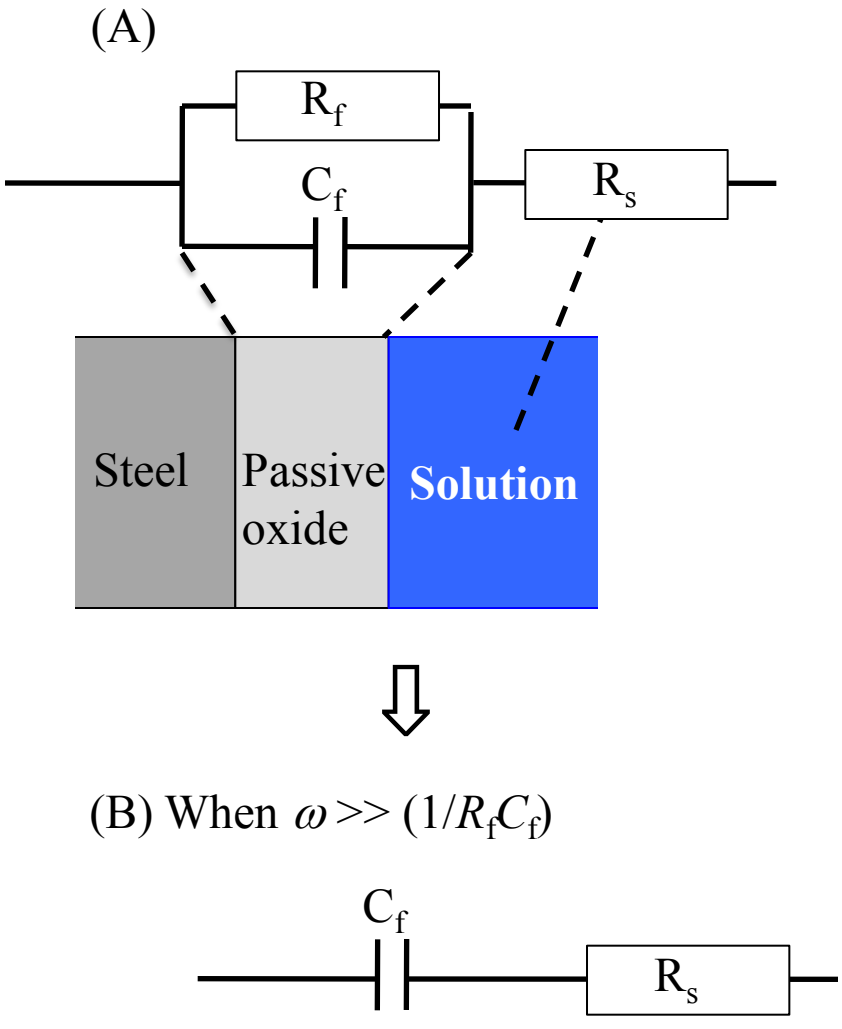
(A)
R_f
C_f
R_s
Steel
Passive oxide
Solution
(B) When $\omega >> (1/R_fC_f)$
C_f
R_s

Fig. 8

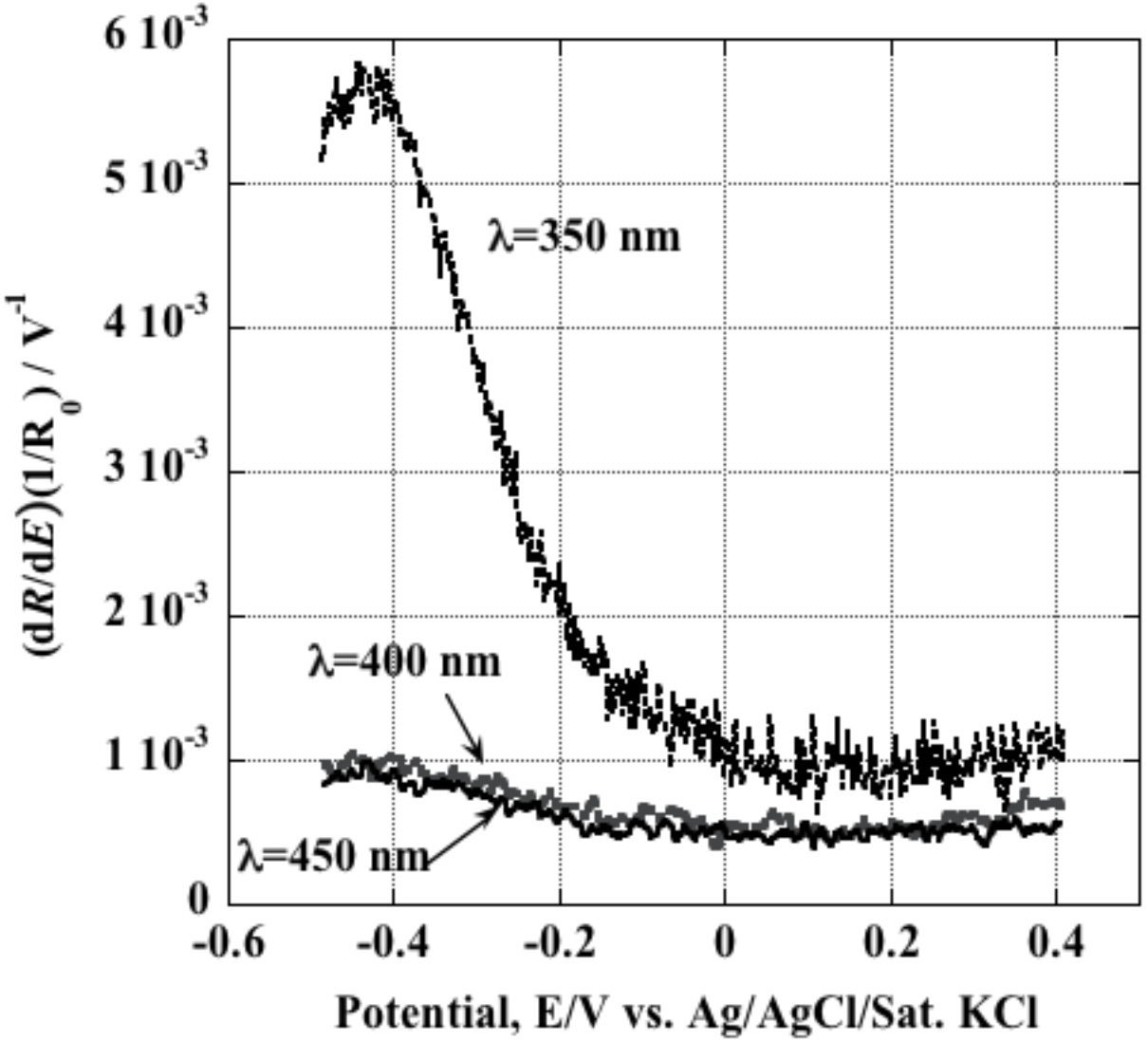
6 10-3
5 10-3
4 10-3
3 10-3
2 10-3
1 10-3
0
(dR/dE)(1/R0) / V-1
λ=350 nm
λ=400 nm
λ=450 nm
-0.6
-0.4
-0.2
0
0.2
0.4
Potential, E/V vs. Ag/AgCl/Sat. KCl

Fig. 9.

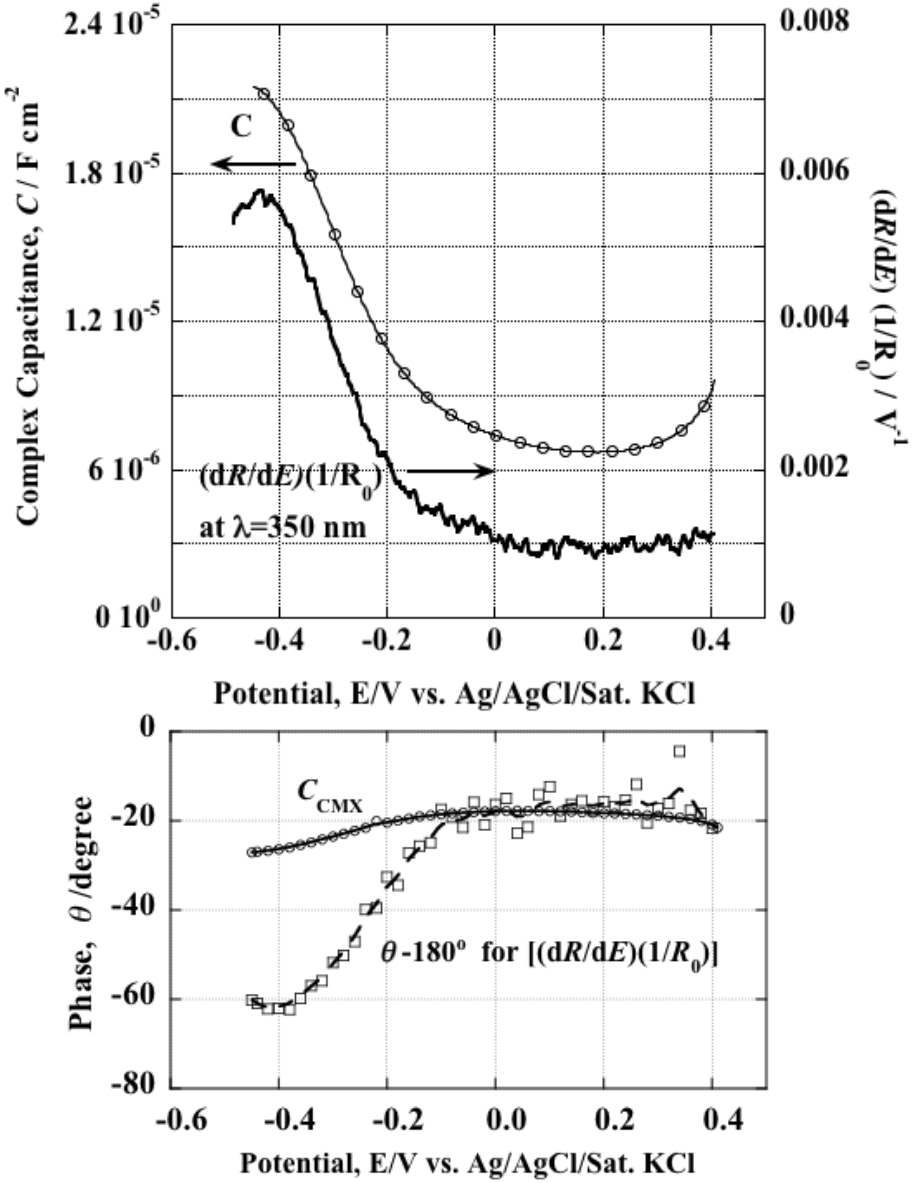
Complex Capacitance, C / F cm-2
2.4 10-5
1.8 10-5
1.2 10-5
6 10-6
0 100
C
(dR/dE)(1/R0)
at λ=350 nm
0.008
0.006
0.004
0.002
0
(dR/dE) (1/R0) / V-1
-0.6
-0.4
-0.2
0
0.2
0.4
Potential, E/V vs. Ag/AgCl/Sat. KCl
Phase, θ /degree
0
-20
-40
-60
-80
CCMX
θ -180° for [(dR/dE)(1/R0)]
-0.6
-0.4
-0.2
0.0
0.2
0.4
Potential, E/V vs. Ag/AgCl/Sat. KCl

Fig. 10

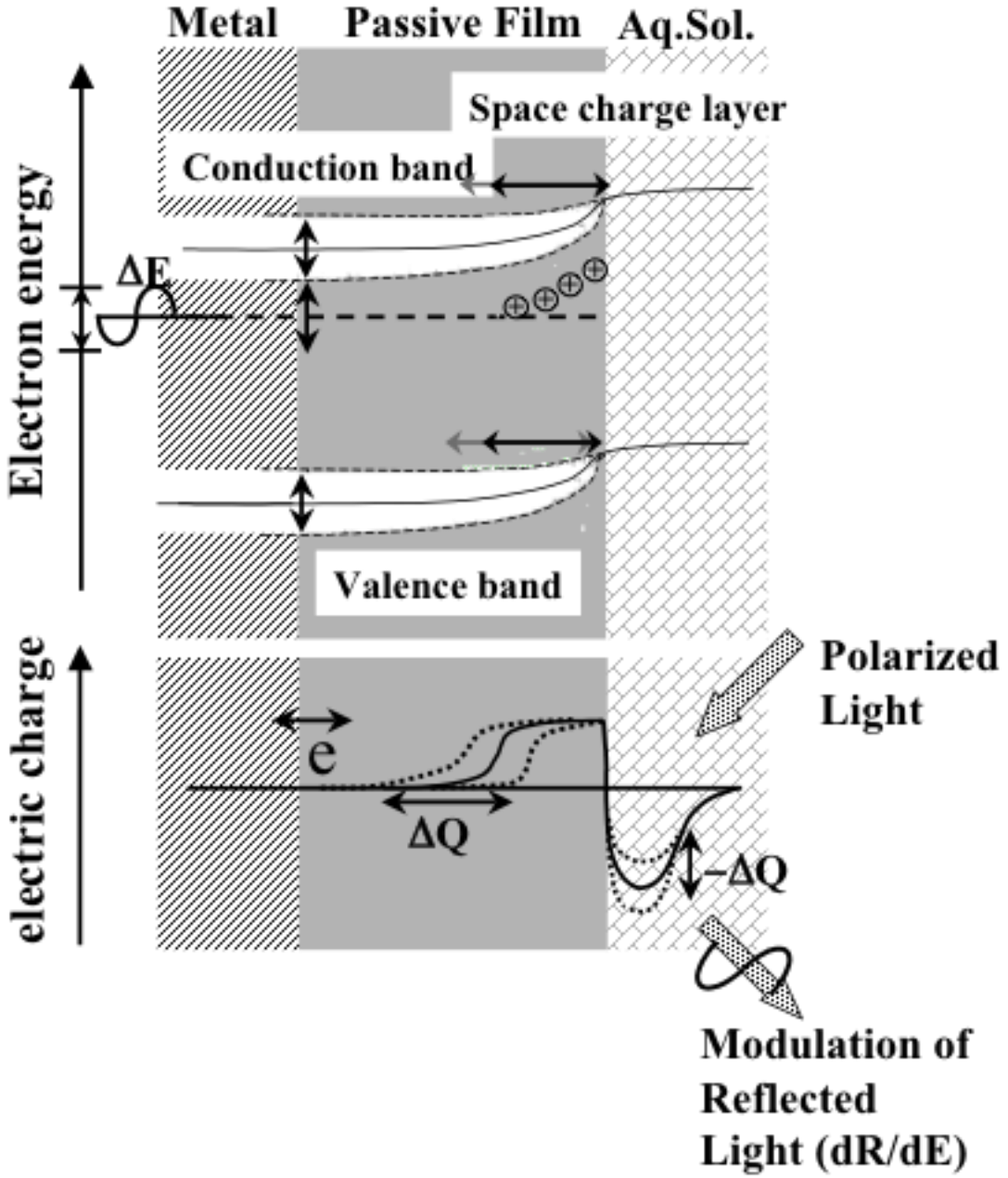
Metal
Passive Film
Aq.Sol.
Space charge layer
Conduction band
Electron energy
ΔE
Valence band
electric charge
e
ΔQ
-ΔQ
Polarized Light
Modulation of Reflected Light (dR/dE)

Fig. 11.

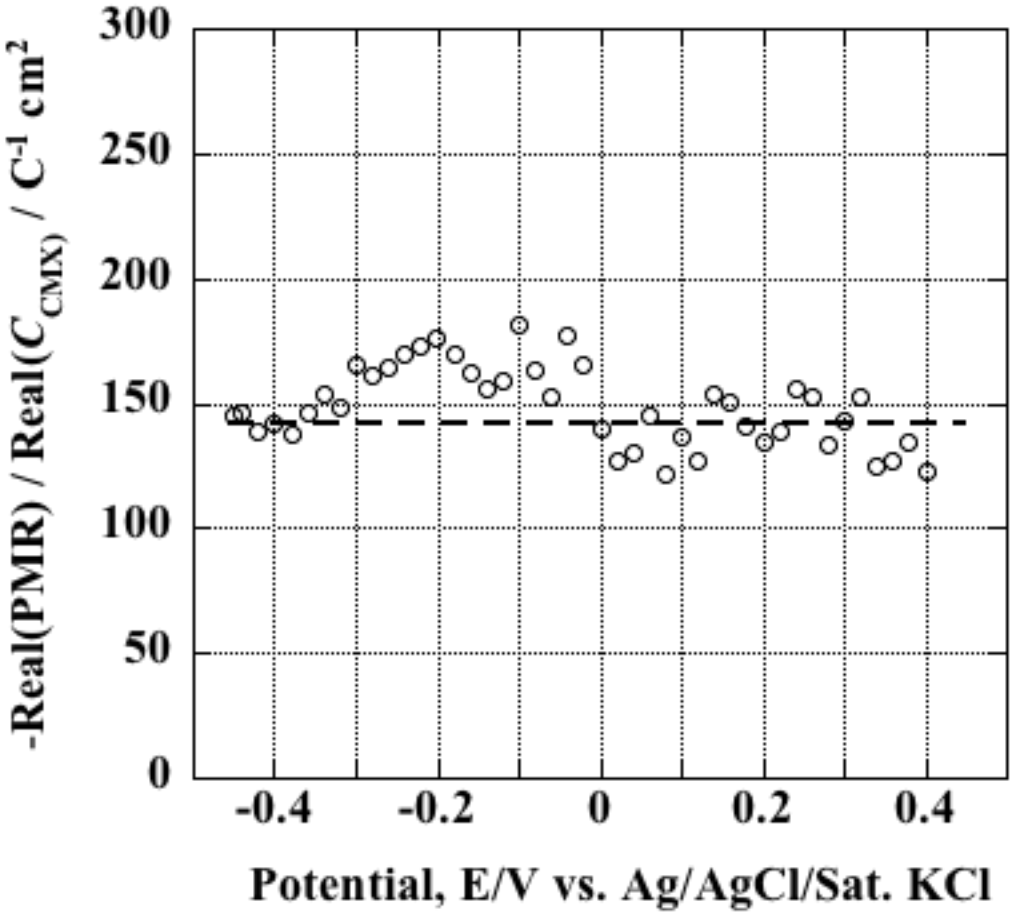
300
250
200
150
100
50
0
-0.4
-0.2
0
0.2
0.4
-Real(PMR) / Real(C_{CMX}) / C^{-1} cm^2
Potential, E/V vs. Ag/AgCl/Sat. KCl

Fig. 12

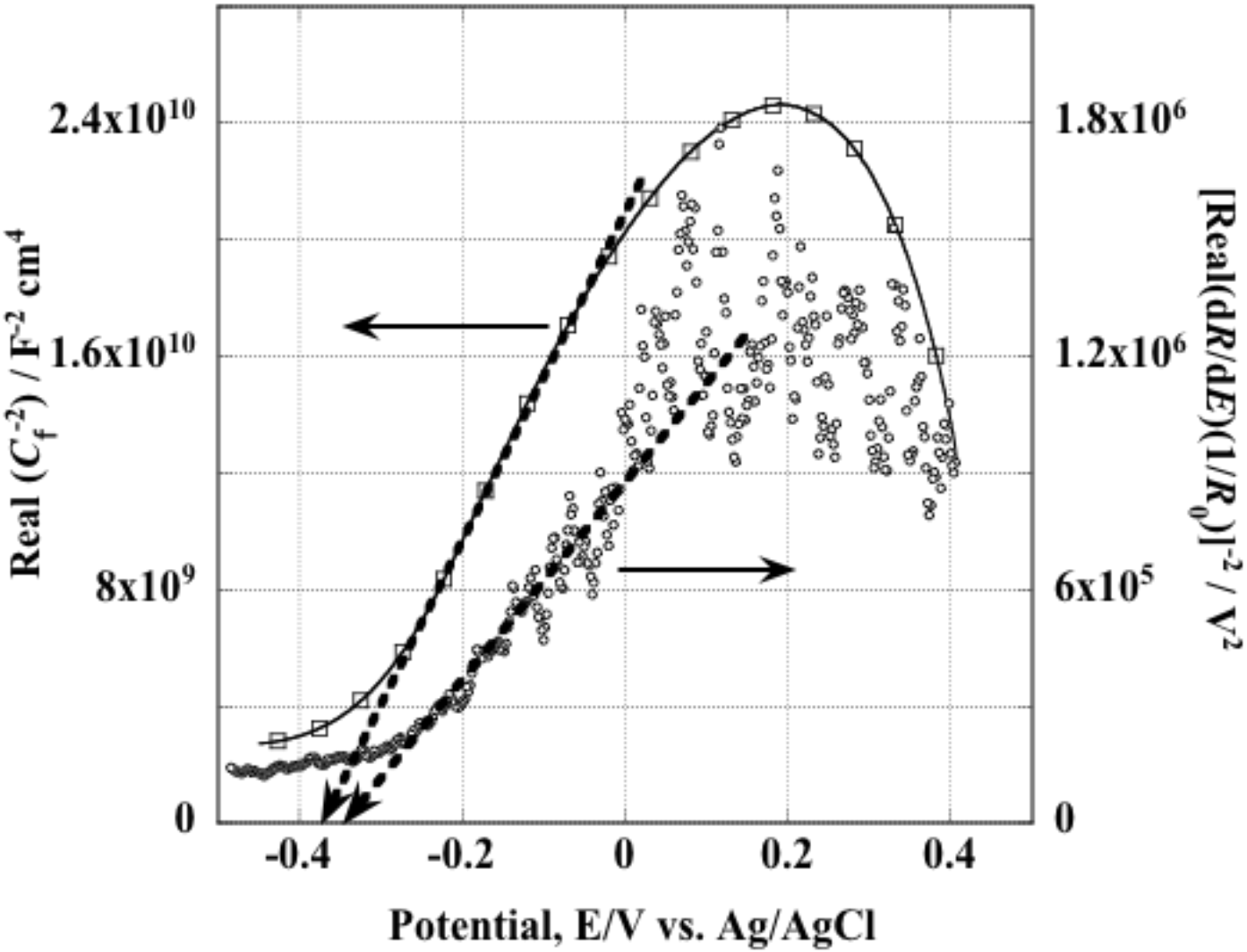
2.4x10^10
1.6x10^10
8x10^9
0
Real (C_f^-2) / F^-2 cm^4
1.8x10^6
1.2x10^6
6x10^5
0
[Real(dR/dE)(1/R_0)]^-2 / V^2
-0.4
-0.2
0
0.2
0.4
Potential, E/V vs. Ag/AgCl

Fig. 13.